25-29 August 2024
inter.noise
NANTES FRANCE

Acoustic Black Hole silencers for broadband dissipation in ducted geometries

Teresa Bravo[1]
Institute for Physical and Information Technologies (ITEFI)
Spanish National Research Council (CSIC)
Serrano 144, 28006 Madrid, Spain

Cédric Maury[2]
Laboratory of Mechanics and Acoustics (LMA CNRS UMR 7031)
4 impasse Nikola Tesla, 13013 Marseille, France

Daniel Mazzoni[3]
Institute of Research on Non-Equilibrium Phenomena (IRPHE CNRS UMR 7342)
49 rue Frédéric Joliot-Curie, 13013 Marseille, France

Muriel Amielh[4]
Institute of Research on Non-Equilibrium Phenomena (IRPHE CNRS UMR 7342)
49 rue Frédéric Joliot-Curie, 13013 Marseille, France

ABSTRACT

The design of novel absorbers avoiding the use of porous or fibrous materials for ventilation and air-conditioning systems constitutes a challenging issue. Recently, the development of metamaterials has provided new noise control perspectives for this problem. Traditional Acoustic Black Holes (ABHs) have been derived with close-ended configurations to achieve broadband absorption. These solutions are suitable as anechoic termination but they cannot be used as silencer as they require a mean flow going through the axis of the acoustic treatment. In this study different configurations of opened ABHs will be considered. Nominal ABHs build on straight cavities of increasing depth along the axial direction. To extend the bandwidth of acoustic performance towards the low frequencies, two different types of ABH silencers will be studied. Cavities with coiled geometries will be considered as a first instance, while the entrance of these cavities will be covered by micro-perforated consequently. The transfer matrix formulation will be adapted to these configurations and used to provide the ABH acoustical performance in terms of reflection and transmission of the silencer to find out the best configuration. These results will be validated against a Finite Element method and experiments will be carried out for the nominal configuration.

[1]teresa.bravo@csic.es
[2]cedric.maury@centrale-marseille.fr
[3]daniel.mazzoni@centrale-marseille.fr
[4]muriel.amielh@univ-amu.fr

1. INTRODUCTION

Many control situations in real life have to face the difficulties associated to the dissipation of low-frequency broadband noise. The integration of proposed solutions into spaces with constraints in total size and cost constitutes a recursive challenge in acoustics [1]. Problems related with ducted configurations have progressively increased its importance due to the nuisance associated to heat, ventilation and cooling duct systems responsible of low-frequency noise emissions at the discharge. Although current treatment designs are able to meet noise reduction policy requirements, further effort should be made in the future as the amount of mechanical ventilation and conditioning system is expected to exponentially increase in the following 30 years [2].

Similar constraints appear in the field of aeronautics, where noise suppression within the engine ducts, at both inlet and exhaust is necessary to meet certification levels. Acoustic treatments traditionally used are constituted of liners made up of a honeycomb core bonded to a perforated sheet in contact with the flow. However, new architectures of Ultra-High Bypass Ratio turbofans imply a lower blade passing frequency and a shorter nacelle with a reduced acoustic treatment surface that can only be efficient by the development of other low noise technologies. The amount of required noise suppression often establishes the length of the required duct treatment. Because duct lengths should be as short as possible to limit total size, classical porous or fibrous materials present limited applications [3] and resonant-type absorbing materials have been proposed.

The use of single-layer micro-perforated partitions [4] constitutes single degree of freedom solutions being effective for around two octaves. For widest bandwidth performance serial and parallel multi-layers partitions can be used with an important increase in total volume. Additionally, acoustic properties of these resonators can enter into the non-linear regime for typical dimensions of holes diameter, that makes resistance and reactance vary with the amplitude of the source [5]. A more controlled treatment is desirable for a simplified problem. In addition, it is important that the selected acoustic treatment presents the appropriate dissipation characteristics over the required frequency range. The key design parameter is the surface impedance of the control device that sets a design criterion to be met for the frequency band of concern. In many cases, the resistance increases progressively with frequency whereas reactance is close to zero and becomes negative with increasing frequency [6]. Optimal properties can only be achieved over a limited range of frequency for single or double degree of freedom partitions. As turbofans engines have strong tonal content in the noise spectrum the design problem is usually limited to the fan fundamental one or two higher harmonics.

Acoustic metamaterials have been explored as good candidates for the control of broadband low frequency noise [7] considering the “slow-sound” effect. Due to the presence of an acoustic device that presents a progressive variation in the geometry or the physical properties, it is possible to gradually slow down the velocity of the incident wave. This idea was first conceived for the passive control of vibrations in thin structures. Initial investigations considered flexural waves propagating in a beam [8], with a thickness progressively decreasing to zero following a power law decay. This provided a termination where the flexural waves are dissipated avoiding reflection from the beam end. From these initial results, many works have considered the reduction of vibrations for different applications [9].

Following the same physical principles, acoustic black holes (ABHs) for noise control applications have also been studied [10-12]. One of the first physical implementations included a set of rings with an inner radius progressively decreasing along the duct axial propagation direction with linear or quadratic profiles totally closed at the end [13]. They verified that the quadratic profile variation provided better absorption results that the linear one. The Transfer Matrix Method (TMM) [14] constitutes an analytical prediction that has been widely used for estimation and optimization of the profiles and distribution of the absorption materials in ABHs[15]. These have to be included to improve the band absorption performance.

Widely-opened ABHs have been studied lately for the study of flow-compliant problems, where both absorption and transmission have to be considered to ensure optimal dissipation inside the metamuffler [16]. This can be achieved when respecting a ratio between the inlet and outlet radii greater than 10. Periodic distributions of symmetric cavities with increasing cavity depth have been used as retarding structures due to the individual resonances and the interaction between adjacent cells. Using a causal optimization methodology [17,18] for the selection of the wall porosity, a 40 dB attenuation and a low reflection can be achieved over a wide bandwidth extending between 1382 Hz and the first duct cut-on frequency at 2038 Hz [18]. However, it is difficult to improve performance towards the low frequency range considering constraints related to total size and weight.

In this study we would like to compare two different strategies to improve low-frequency broadband dissipation while maintaining a constant ABH axial length. We will first study a coiled ABH type silencer (C-ABH) where cavities are filled with coiled channels extended along the cavity thickness. The second strategy is achieved by placing micro-perforated facings at the entrance of the ABH cavities (MPP-ABH). In the following section the main equations governing the behavior of the different ABHs will be analytically outlined using a description in terms of the Transfer Matrix Method (TMM). The acoustic performance of the three different configurations will be compared in Section 3 against a numerical Finite Element Method (FEM) presenting a parametric study in terms of the main characteristics influencing dissipation inside the ABH. Finally, an experimental set-up is presented for the validation of the predicted results. We will finish with the main conclusions and some ideas for continuation of the work.

2. THEORETICAL ANALYSIS

The physical configurations of the proposed coiled and MPP metamufflers are presented in Figure 1.

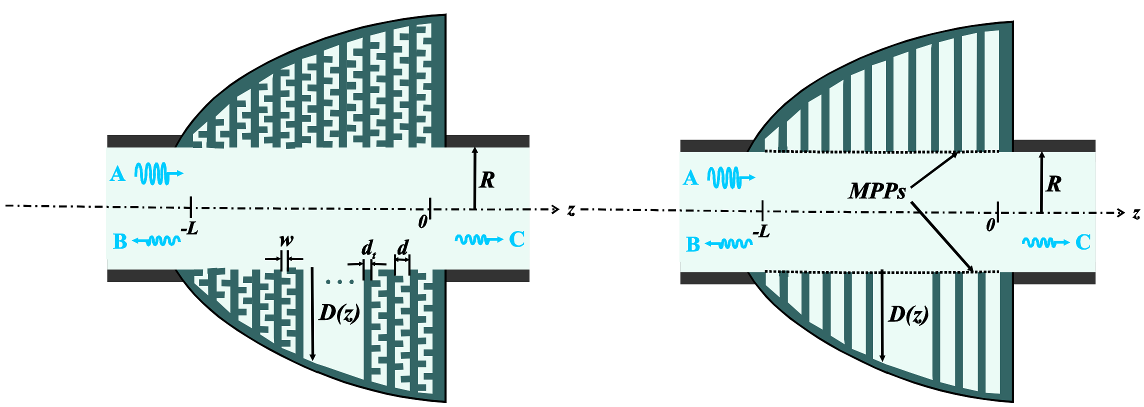

Figure 1: Sketch of the coiled ABH (C-ABH) (left) and the MPP-ABH (right) silencers.

The basic arrangement is composed of a fully-opened ABH silencer of radius R and length L with a finite number N of cavities of width d separated by thin walls and a varying cavity depth D_i [18]. Introducing coiled channels inside the cavities increases the path length for the ith coiled cavity by a quantity $D_{c,i} = (D_i/2)(1+d/w)$ with w ($<d$) the width of the coiled channel, as indicated in Figure 1.

The second configuration assumes that the entrance of the cavities are covered by a micro-perforated panel denoted as MPP-ABH. Assuming a frequency dependence as $e^{+i\omega t}$, the overall transfer impedance has been provided by Maa [4] and takes the expression

$$\frac{Z_{\mathrm{MPP}}}{\sigma} = \frac{32\eta\, t_h}{\sigma d_h^2}\left[\sqrt{1+\frac{k_h^2}{32}} + \frac{\sqrt{2}}{32}k_h\frac{d_h}{t_h}\right] + \mathrm{j}\rho_0\omega\frac{t_h}{\sigma}\left[1+\left(9+\frac{k_h^2}{2}\right)^{-\frac{1}{2}} + \frac{8}{3\pi}\frac{d_h}{t_h}\right], \qquad (1)$$

where d_h is the MPP circular holes diameter, t_h is the panel thickness, σ is the perforation radio, η the dynamic viscosity of the air, and $k_h = (d_h/2)/r_{\mathrm{visc.}}(\omega)$, the perforate constant, e.g. the ratio of the hole radius to the viscous boundary layer thickness, $r_{\mathrm{visc.}}(\omega) = \sqrt{\eta/\rho_0\omega}$, with ρ_0 the air density.

The linearized mass conservation equation when considering plane wave propagation confined within a cylindrical geometry fitted with an ABH with infinite cavities can be expressed as [19]

$$\frac{\partial v_z}{\partial z} + \frac{v_n}{r_H} + \frac{\mathrm{d}(\log S)}{\mathrm{d}z}v_z = -\frac{\mathrm{j}\omega}{\rho_0 c_0^2}p, \quad -L < z < 0 \qquad (2)$$

with v_z the axial velocity component, $v_n = p/Z$ the normal velocity over the boundary $\Sigma(r = R, -L < z < 0)$ and p the acoustic pressure. $r_H = S/U$ is the hydraulic radius with S the cross-sectional area of the duct and U the circumference of the lining. Substituting in Eq. (2) the linearized momentum conservation equation, $-\mathrm{j}\omega\rho_0 v_z = \partial p/\partial z$, one obtains in plane wave regime a propagation equation

$$\frac{\mathrm{d}^2 p}{\mathrm{d}z^2} + k_0^2\left[1 - \mathrm{j}\frac{y(z)}{k_0 r_H}\right]p = 0, \qquad (3)$$

where $y = Z_0/Z$ is the wall specific admittance normalized by $Z_0 = \rho_0 c_0$ the fluid characteristic impedance with c_0 the sound speed. When considering a continuous distribution of annular cavities with axially varying depth $D(z)$, the wall-admittance neglecting visco-thermal losses in the cavities is given by [18]

$$y(z) = -\mathrm{j}\frac{J_1(k_0R)H_1[k_0(R+D(z))] - J_1[k_0(R+D(z))]H_1(k_0R)}{J_0(k_0R)H_1[k_0(R+D(z))] - J_1[k_0(R+D(z))]H_0(k_0R)}. \qquad (4)$$

The Transfer Matrix Method (TMM) is an analytical approach that has been used for prediction of acoustic performance of the ABH muffler composed of a finite number of cavities, with an axial variation of the cavity depth. To calculate the acoustic performance of the fully-opened ABH, continuity conditions on the acoustic pressure $(p_i = p_{i+1})$ and acoustic flow rate $(u_i = (p_{i+1}/Z_{cav}) + u_{i+1})$ at the ith cavity-ring , we obtain a relationship between the input and output quantities at the interface $[p_i \ u_i]^{\mathrm{T}} = \mathbf{T}_i[p_{i+1} \ u_{i+1}]^{\mathrm{T}}$, related by the associated transfer matrix that takes the expression

$$\mathbf{T}_i = \begin{bmatrix} \cos(k_0 d) & \mathrm{j}\dfrac{Z_0}{S}\sin(k_0 d) \\ \mathrm{j}\dfrac{S}{Z_0}\sin(k_0 d) & \cos(k_0 d) \end{bmatrix} \begin{bmatrix} \cos(k_0 d_t) & \mathrm{j}\dfrac{Z_0}{S}\sin(k_0 d_t) \\ \mathrm{j}\dfrac{S}{Z_0}\sin(k_0 d_t) & \cos(k_0 d_t) \end{bmatrix} \begin{bmatrix} 1 & 0 \\ Y_{\mathrm{cav},i} & 1 \end{bmatrix}, \tag{5}$$

with $Y_{\mathrm{cav},i} = S_{\mathrm{cav}}\, y(z_i)/Z_0$ the localized side-branch volume admittance and $S_{\mathrm{cav}} = 2\pi R d$ the cavity entrance area. Considering that the cavity can be mounted directly on the duct or shielded from the duct by a micro-perforated lining, $Y_{\mathrm{cav},i}$ can take the following expression in the low-frequency limit

$$Y_{\mathrm{cav},i} = \begin{cases} \mathrm{j}\dfrac{k\pi d}{Z_0}\left[(R + D_{c,i})^2 - R^2\right] & \text{without MPP} \\ c_0\left[\dfrac{Z_{Maa}}{S_{\mathrm{cav,i}}} - \mathrm{j}\dfrac{Z_0}{k\pi d\left[(R + D_i)^2 - R^2\right]}\right]^{-1} & \text{with MPP.} \end{cases} \tag{6}$$

For the coiled ABH we need to consider only the first expression from Equation (6), $Y_{\mathrm{cav},i} = \mathrm{j}\dfrac{k\pi d}{Z_0}\left[(R + D_{c,i})^2 - R^2\right]$. Without coiling ($w = d$), one retrieves $D_{c,i} = D_i$ and recover the basic fully-opened ABH configuration. The total transfer matrix between the ABH inlet and outlet, is calculated as the product of all the sub-matrices associated to each unit as

$$\mathbf{T} = \prod_{i=1}^{N} \mathbf{T}_i = \begin{bmatrix} T_{11} & T_{12} \\ T_{21} & T_{22} \end{bmatrix}. \tag{7}$$

When imposing the continuity conditions between the input and output of the metamuffler, $(p_{N+1} = Z_0 u_{N+1}/S)$, we can obtain the expressions for the reflection and transmission coefficient in terms of the particular elements of the overall transfer matrix as

$$\begin{cases} r = \dfrac{(T_{11} + z_0 T_{12}) - (T_{21} + z_0 T_{22})}{(T_{11} + z_0 T_{12}) + (T_{21} + z_0 T_{22})} \\ t = \dfrac{1 + r}{T_{11} + z_0 T_{12}}, \end{cases} \tag{8}$$

with $z_0 = S/Z_0$.

3. ANALYTICAL PREDICTIONS

Simulations have been performed from the TMM and from the FEM Visco-Thermal Acoustics models to calculate the acoustical performance of fully-opened ABH-type silencers of radius $R = 0.047\,\mathrm{m}$, length $L = 0.1\,\mathrm{m}$ and made up of $N = 15$ cavities with an axial depth increasing quadratically at a rate $m = 2$. Three types of configurations have been examined:

- An ABH silencer with straight cavities of width $d = 4.7\,\mathrm{mm}$, separated by walls of thickness $d_t = L/N - d = 2\,\mathrm{mm}$.
- A MPP-ABH silencer with straight cavities covered at their mouth by a MPP with holes diameter $d_h = 0.5\,\mathrm{mm}$, perforation ratio $\sigma = 8.1\%$ and thickness $t = 1.5\,\mathrm{mm}$.
- A C-ABH silencer with cavities coiled by channels of width $w = 2.5\,\mathrm{mm}$.

The geometrical parameters of the ABH silencers can be seen in Figure 1. Figure 2 examines the influence of two approaches to broaden the high-dissipation and impedance matching performance of ABH-silencers towards low-frequencies: covering the cavity mouths by a MPP (red curves) or coiling the cavity channels (blue curves). The black reference curves are related to an ABH silencer with straight cavities. Such ABH silencer achieves almost full dissipation as from 1400 Hz up to the duct cut-on frequency 2143 Hz, as seen from Figure 2(a). It also achieves a trend towards impedance matching, i.e. unit resistance and zero reactance, as from 1400 Hz, with some under-damped cavity resonances above 1800 Hz, as shown by Figure 2(b).

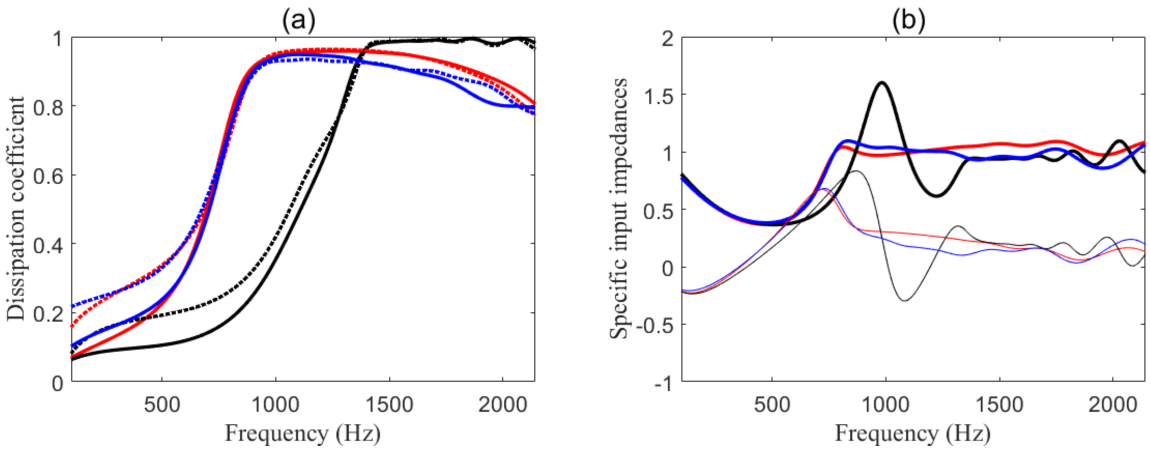

Figure 2: (a) the dissipation coefficient spectra related to the ABH (black thick: TMM, black dots: FEM), to the MPP-ABH (red thick: TMM, red dots: FEM) and to the C-ABH (blue thick: TMM, blue dots: FEM); (b) the specific input impedances (thick: resistance, thin: reactance) at the entrance of the ABH (black), the MPP-ABH (red) and the C-ABH (blue) silencers.

It can be seen from Figure 2(a) that both MPP and coiling approaches provide high dissipation values, that stay between 0.8 and 0.96 over a wide bandwidth that starts from 1000 Hz up to 2143 Hz. Figure 2(b) shows that their specific input impedance tends to match unity, i.e. that of a plane wave propagating in an infinite duct, as from 900 Hz, with a lower resistance of the MPP-ABH with respect to the C-ABH above 1200 Hz, resulting in slightly lower dissipation performance over this frequency range.

For the three types of silencers, Figures 2 and 3 show that the ABH effect is characterized by high dissipation, low reflection (lower than 0.02), low transmission and impedance matching over a wide bandwidth, extended towards low frequencies by MPP shielding or coiling the cavities. These approaches bring further reactance, either by the effective mass added though the MPP holes or by the cavity stiffness reduced when increasing the acoustical path length in the coiled cavities.

These trends simulated by the TMM are well predicted by the FEM over the silencer efficiency range where the dissipation tends to be prominent in the locally resonant cavities. These locally activated cavities lead to less inter-resonator coupling, compatible with the TMM assumption (plane wave propagation and no evanescent waves). More discrepancies are observed at low frequencies between the TMM and the FEM. These correlation properties between TMM and FEM can also be seen in Figures 3(a) and (b) for the reflection and transmission properties of the ABH silencers.

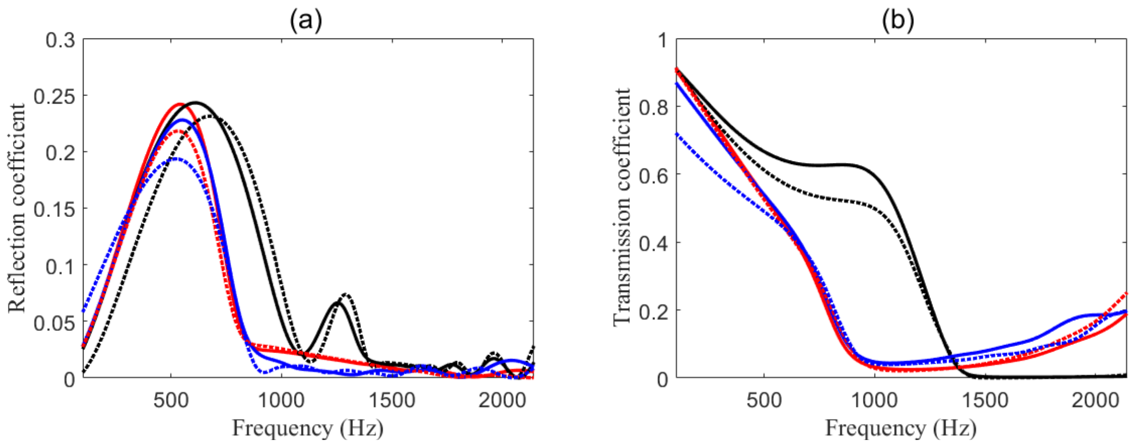

Figure 3: The reflection (a) and transmission (b) coefficient spectra related to the ABH (black thick: TMM, black dots: FEM), to the MPP-ABH (red thick: TMM, red dots: FEM) and to the C-ABH (blue thick: TMM, blue dots: FEM).

Figure 4 shows the sound pressure levels (SPL) distribution calculated by FEM for the three types of ABH silencers at the onset of their efficiency range: 1400 Hz for the reference ABH silencer [Figure 4(a)] and 1000 Hz for the MPP-ABH and C-ABH silencers [Figures 4(b) and (c)]. A progressive drop of the SPLs is observed between the inlet and outlet of the silencers with continuity of the pressure over the cavity mouths, except for the MPP-ABH due to the jump of pressure across the MPP. This is accompanied by a distortion of the acoustical wave front towards the cavity mouth, more visible for the ABH and C-ABH cavities. At 1400 Hz (resp. 1000 Hz), the deepest cavity of the ABH (resp. C-ABH) silencer is resonant. It is associated to a minimum pressure and maximum radial velocity at the mouth of these cavities at its quarter- wavelength resonance frequencies. The MPP-ABH cavity resonances are of Helmholtz-type. It was found that the resonance of the deepest cavity covered by the MPP is activated at 850 Hz, below 1000 Hz, the onset of the high-dissipation plateau. However, its wide bandwidth (due to the MPP added resistance) and merging with the neighboring closely-packed resonances of the deepest cavities enables to achieve a smooth rise of the dissipation curve up to the plateau value, as seen from Figure 2(a).

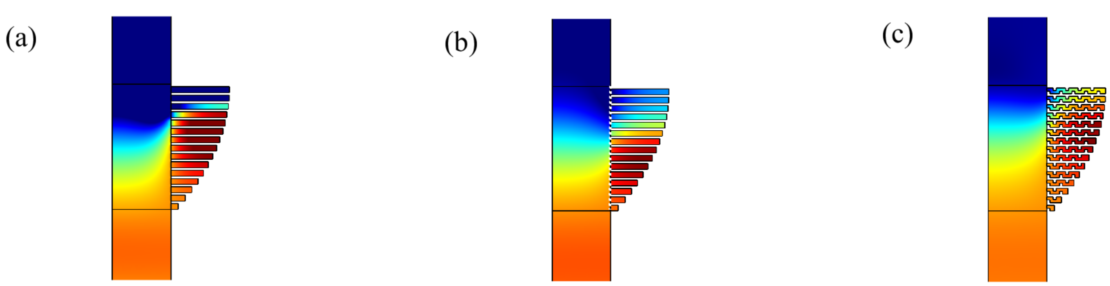

Figure 4: SPLs (dB) calculated by FEM within the ABH at 1400 Hz (a), the MPP-ABH at 1000 Hz (b) and the C-ABH at 1000 Hz (c); white dots in (b) show the MPP location at the cavity mouths; the colors scale from 74 dB (dark) to 95 dB (bright).

Figure 5 shows the effect of increasing the MPP holes diameter d_h on the acoustical performance of the MPP-ABH silencer. Since the holes interspacing Λ is kept at a fixed value $\Lambda = d/3 = 1.6$ mm, increasing d_h also increases the perforation ratio $\sigma = \pi d_h^2/(4\Lambda^2)$. Small values of the MPP holes diameter down to 0.2 mm is accompanied by an increase of the MPP reactance and a decrease of the MPP resistance by a factor 4 with respect to those related to the largest MPP holes diameter. As a consequence, it results in a downshift of the maximum dissipation frequency down to 700 Hz, but also a lowering and broadening of the dissipation hump [Figure 5(a), thin red curve]. This is accompanied by minute reflections and very large transmission values [Figures 2(b) and (c)]. In the limit of very low d_h, the MPPs rigidly obstruct the cavity mouths and one obtains a simple rigid duct with near-zero dissipation (still that associated to the visco-thermal boundary layer at the duct walls), zero reflection and full transmission.

On the other hand, if one increases the MPP holes diameter up to their largest value, close to one third of the cavity width, one observes an ABH effect with near-unit dissipation together with minute reflection and transmission over a wide bandwidth whose onset increases with d_h up to 1300 Hz [Figure 2, dashed curves]. As the MPP holes diameter d_h tends to one third of the cavity width , $d/3$, the performance of the MPP-ABH silencer get closer, but does not reach that of the ABH silencer without MPP.

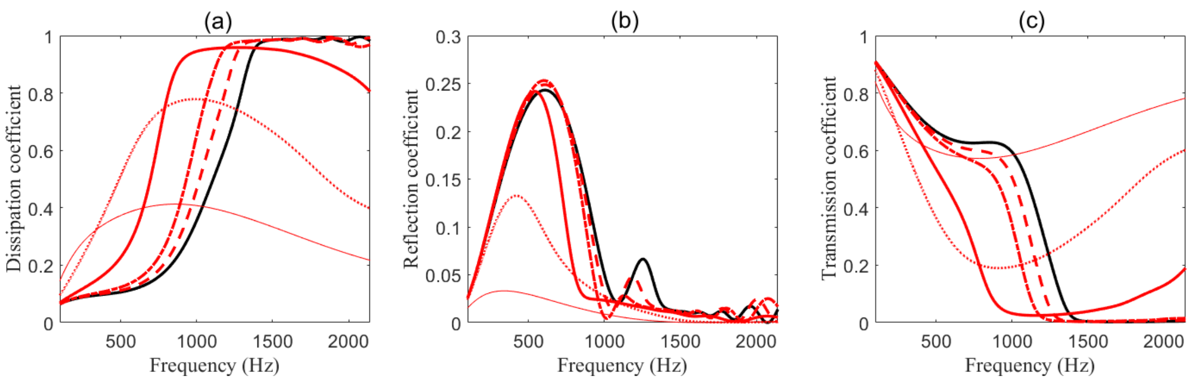

Figure 5: The dissipation (a), reflection (b) and transmission (c) coefficients related to the ABH silencer (black) and to the MPP-ABH when increasing the MPP holes diameters (thin: $d_h = 0.2$ mm, $\sigma = 1.3\%$; dots: $d_h = 0.3$ mm, $\sigma = 2.3\%$; thick: $d_h = 0.5$ mm, $\sigma = 8.1\%$; dash-dotted: $d_h = 1$ mm, $\sigma = 32\%$; dashed: $d_h = 1.59$ mm, $\sigma = 83\%$), all simulated by the TMM.

Overall, it appears that holes diameter (resp. perforation ratio) greater than 0.5 mm (resp. 8.1%) are required to generated an ABH effect when coating the silencer cavity, but their optimal values have to be found not to restrict too much the ABH bandwidth. As they cross-couple with other geometric parameters of the ABH silencer, a global optimization process is then required.

Figure 6 shows the effect of increasing the width w of the coiled channels on the acoustical performance of the C-ABH silencer. As seen in Figure 1, coiling the acoustical path length in each cavity is achieved by inserting inner protrusions of thickness and spacing assumed to be equal to the width w of the channel meandering around the protrusions. A coiling factor can then be defined, $\beta = 0.5(1 + d/w)$, that increases when w decreases, and that represents the relative increase in the acoustical path length induced by the coiling. Decreasing w from $w = d$ ($\beta = 1$, no coiling) down to $w = d/9.4$ ($\beta = 5.2$, high coiling) decreases the effective air stiffness in the cavities, downshifts the first quarter-wavelength resonance frequencies due to a longer acoustical path length in the coiled channels. It also increases the input resistance at the channel slits. Consequently, Figure 6(a) shows that the near-constant dissipation values resulting from merging between the C-ABH channels resonances has a bandwidth substantially extended towards the low-frequencies, but at the expense of reduced maximum dissipation values. Figures 6(b) and (c) show that it is followed by very low reflection and very large transmission values. In the limit of zero-channel width, one gets a simple rigid duct.

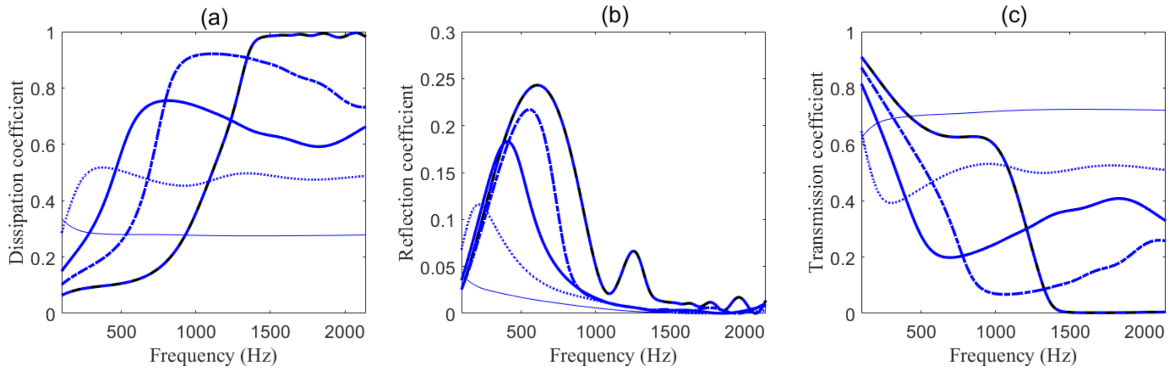

Figure 6: The dissipation (a), reflection (b) and transmission (c) coefficients related to the ABH silencer (black) and to the C-ABH when increasing the coiled channel width (thin: $w = 0.5$ mm ; dots: $w = 0.9$ mm ; thick: $w = 1.6$ mm ; dash-dotted: $w = 2.3$ mm ; dashed: $w = 4.7$ mm), all simulated by the TMM.

From Figure 6 we can conclude that the reflection values are favorably sensitive to channel coiling (they decrease when the coiling increases), but the maximum dissipation and minimum transmission performance degrade when increasing the coiling, although they occur at lower frequencies. Once again, an optimal value of the channel coiling factor is required to recover a broadband plateau of high dissipation values, but this has to be achieved in conjunction with the other C-ABH geometrical parameters.

4. EXPERIMENTAL ANALYSIS

Experiments have been performed on an acoustic test bench in order to characterize the acoustic performance of the MPP-ABH silencer, displayed in Figure 7.

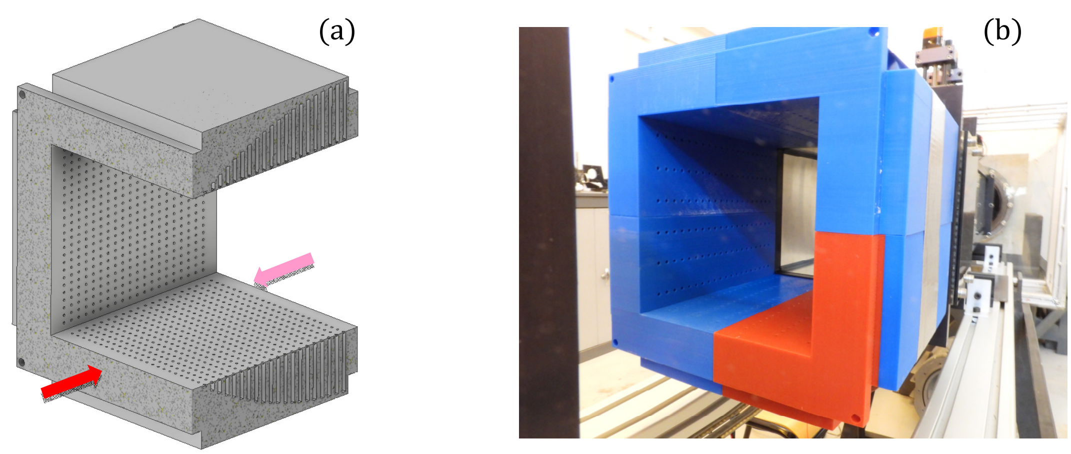

Figure 7: (a) Cross-sectional view of the MPP-ABH silencer with progressive (red) and regressive (magenta) plane wave excitations; (b) Inner view of the 3D-printed MPP-ABH silencer, from the outlet side, mounted on a two-source rectangular acoustic test bench.

The ABH-SPC silencer has been manufactured from fused deposition modelling out of ABS polymer. It is located between two rigid duct sections, 1 m long with cross-sectional area $H \times W = 0.15 \times 0.15\,\mathrm{m}^2$. It has a length $L = 0.15\,\mathrm{m}$ and is filled with $N = 20$ cavities of width $d = 0.0035\mathrm{m}$ separated by walls of thickness $d_t = 0.004\,\mathrm{m}$. The cavity mouths are covered by a perforated interface of thickness $0.0015\,\mathrm{m}$ with circular holes diameters $d_h = 0.0026\,\mathrm{m}$ and pitches $u_z = 0.0075\mathrm{m}$ (resp. $u_y = 0.025\,\mathrm{m}$) along the axial (resp. crosswise) directions. This leads to a perforation ratio $\sigma = 2.8\,\%$.

The two-source and three-microphone method has been used to determine the scattering matrix of the MPP-ABH silencer, as detailed in [20] with a passive test device. Independent acoustic states were generated by two compression drivers driven by white noise signal and located on either side at 0.8 m of the silencer. Transfer functions were measured between a pair of three surface microphones and the source drive signal. The wall-mounted microphones were located on either side of the silencer and separated from each other by a distance $0.05\,\mathrm{m}$. The outgoing and ingoing plane wave amplitudes generated by the acoustic states were calculated from the measured transfer functions from pseudo-inversion of the propagation matrix.

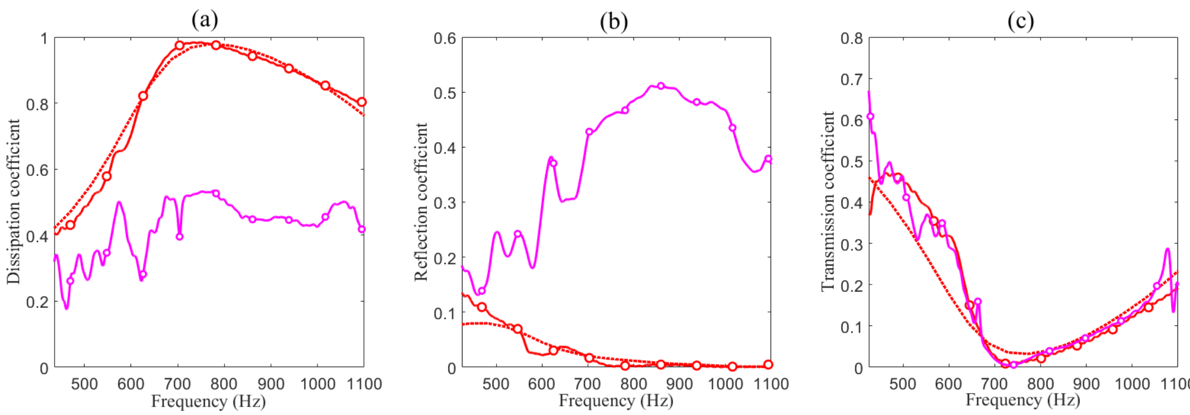

Figure 8: The dissipation (a), reflection (b) and transmission (c) coefficients related to the MPP-ABH silencer assuming progressive (red dots: FEM; red circles: measurements) or regressive (magenta circles: measurements) plane wave excitations.

It can be seen from Figure 8 that the dissipation, reflection and transmission coefficients agree within 7% with the FEM simulations over the silencer efficiency range 700 Hz – 1134 Hz up to the duct cut-on frequency. Over this broad bandwidth, the dissipation coefficient stays greater than 0.8 and the reflection (resp. transmission) coefficients do not exceed 0.02 (resp. 0.2) respectively. The perforated coating with low porosity essentially brings added reactance that shifts the ABH efficiency range from 1400 Hz – 2120 Hz without coating (not shown) down to 700 Hz – 1134 Hz. A non-flat dissipation spectrum is observed in Figure 8(a). An optimization of the MPP-ABH parameters would be required to recover a flat dissipation spectrum in plane wave regime as from 700 Hz.

It is of interest to observe from Figure 8 that the ABH effect vanishes if the incident wave is regressive. Indeed, a reflection bump is observed in Figure 8(b) that reaches 0.5 towards 850 Hz. This is due to the wall-impedance mismatch when the incident wave impinges onto the silencer deepest cavities when they are resonant. Meanwhile, the dissipation spectrum in Figure 8(a) is rather flat and hardly exceeds 0.5. Reciprocal transmission is observed in Figure 8(c) between the left-to-right and right-to-left transmission coefficients, despite measurements errors.

5. FINAL COMMENTS AND CONCLUSIONS

Low-frequency control of sound presents unique challenges associated to size and weight limitations in real applications. Considering the emerging metamaterials used as acoustic devices, ABHs have been developed based on the slow-sound effect when an acoustic perturbation propagates along a waveguide. In this work, we have considered a fully-opened ABHs for the study of flow-compliant problems, where both absorption and transmission have to be considered to ensure optimal dissipation. Although good operational values are obtained for the nominal configuration, it is interesting to study alternatives to enhance the dissipation band towards lower frequency values without modifying total size. In this work we have compared two different approaches comprising the use of a micro-perforated lining at the entrance of the ABH cavities, and a coiled ABH where cavities are filled with twisted channels to increase the effective path length.

Analytical and numerical models have been developed to predict the acoustic performance of the fully-opened base configuration, and the coiled and MPP-ABHs. Both alternatives have been shown to be able to displace the high performance lower bound towards the low frequency range although it also implies a slight degradation of the results at the upper frequency bound. However, the results can be further improved considering that the two proposed solutions are tunable devices that can be adjusted by the proper selection of the constitutive physical parameters. In particular, in this work we have studied the effect of the MPP holes diameter and we have outlined the corresponding trade-off between the maximum dissipation values obtained and the performance bandwidth of the MPP-ABH. Concerning the coiled configuration, we have also found a similar trend when considering the coiled channel width. For the selection of the optimal parameters a fully heuristic optimization procedure has to be performed.

Experimental studies were carried out with a micro-perforated ABH using the two-source and three-microphone method to determine the scattering matrix of the MPP-ABH silencer. They have confirmed the improved performance in the low frequency range and the validity of the predictions. Future work can be directed towards the incorporation of a mean grazing flow circulating downstream the waveguide and the effects on the acoustic performance. We are also interested to consider effects on the pressure loss associated to the different ABH wall treatments.

ACKNOWLEDGEMENTS

This work is part of the project TED2021-130103B-I00, funded by MCIN/AEI/10.13039/501100011033 and the European Union “NextGenerationEU”/PRTR, and project PID2022-139414OB-I00 funded by MCIN/ AEI /10.13039/501100011033/ and by "ERDF A way of making Europe". It has also received support from the French government under the France 2030 in-vestment plan, as part of the Initiative d'Excellenced'Aix-Marseille Université - A*MIDEX (AMX-22-RE-AB-157).

REFERENCES

1. C.H. Hansen and Kristy L. Hansen, *Noise Control,* 2nd edition, CRC Press, Taylor and Francis group, London, 2021.
2. IEA, International Energy Agency, Energy Efficiency 2021, https://www.iea.org/reports/energy-efficiency-2021.
3. C. Zwikker and C. W. Kosten, *Sound Absorbing Materials*, Elsevier Press, Amsterdam, 1949.
4. D. Y. Maa, Potential of microperforated panel absorbers, Journal of the Acoustical Society of America, **104**, 2861–2866, 1998.

5. T. Bravo, C. Maury and C. Pinhede, Optimisation of micro-perforated cylindrical silencers in linear and nonlinear regimes, Journal of Sound and Vibration, **363**, 359-379, 2016.
6. M. Abom and S. Sack. Revisiting the Cremer Impedance. Forum Acusticum, Lyon, France, 403-406, 7-11 December 2020.
7. N. Jiménez, V. Romero-García, V. Pagneux, J.-P. Groby, Rainbow-trapping absorbers: Broadband, perfect and asymmetric sound absorption by subwavelength panels for transmission problems, Scientific Reports **7**, 13595, 2017.
8. M. A. Mironov, Propagation of a flexural wave in a plate whose thickness decreases smoothly to zero in a finite interval, Soviet Physics Acoustics **34**, 318–319, 1988.
9. J. Deng, X. Chen, Y. Yang, Z. Qin, W. Guo, Periodic additive acoustic black holes to absorb vibrations from plates, International Journal of Mechanical Sciences **267**, 108990, 2024.
10. B. M. P. Chong, L. B. Tan, K. M. Lim, H. P. Lee, A review on Acoustic Black-Holes (ABH) and the experimental and numerical study of ABH-featured 3D printed beams, International Journal of Applied Mechanics **9**, 1750078, 2017.
11. X. Zhang and L. Cheng. Broadband and low frequency sound absorption by Sonic black holes with Micro-perforated boundaries, Journal of Sound and Vibration **512**, 116401, 2021.
12. A. Mousavi, M. Berggren, L. Hägg, E. Wadbro, Topology optimization of a waveguide acoustic black hole for enhanced wave focusing, Journal of the Acoustical Society of America **155**, 742-756, 2024.
13. A. El Ouahabi, V. Krylov, D. O'Boy, Experimental investigation of the acoustic black hole for sound absorption in air, in Proceedings of the 22nd International Congress on Sound and Vibration, July 12–16, Florence, 2015.
14. O. Guasch, M. Arnela, P. Sánchez-Martín, Transfer matrices to characterize linear and quadratic acoustic black holes in duct terminations, Journal of Sound and Vibration **395**, 65–79, 2017.
15. G. Serra, O. Guasch, M. Arnella, D. Miralles, Optimization of the profile and distribution of absorption material in sonic black holes, Mechanical Systems and Signal Processing **202**, 110707, 2023.
16. Y. Mi, W. Zhai, L. Cheng, C. Xi and X. Yu, Wave trapping by acoustic black hole: Simultaneous reduction of sound reflection and transmission, Applied Physics Letters **118**, 114101, 2021.
17. T. Bravo and C. Maury, Causally-guided acoustic optimization of rigidly-backed micro-perforated partitions: Case studies and experiments Journal of Sound and Vibration, **523**, 116735, 2022.
18. T. Bravo, C. Maury, Broadband sound attenuation and absorption by duct silencers based on the acoustic black hole effect: Simulations and experiments, Journal of Sound and Vibration **561**, 117825, 2023.
19. M. A. Mironov, V. V. Pislyakov, One-Dimensional Acoustic Waves in Retarding Structures with Propagation Velocity Tending to Zero, Acoustical Physics **48**, 347–352, 2002. Translated from Akusticheski Ï Zhurnal, **48**, 115223, 2002.
20. E. Garnell, M. and G. Banwell, The use of the two-port method to characterize high-speed small fans. Applied Acoustics, **146**, 155–163, 2019.